Automatic Identification of Artifact-Related Independent Components for Artifact Removal in EEG Recordings

Yuan Zou, *Student Member, IEEE*, Viswam Nathan, *Student Member, IEEE*, and Roozbeh Jafari, *Senior Member, IEEE*

***Abstract*—Electroencephalography (EEG) is the recording of electrical activity produced by the firing of neurons within the brain. These activities can be decoded by signal processing techniques. However, EEG recordings are always contaminated with artifacts which hinder the decoding process. Therefore, identifying and removing artifacts is an important step. Researchers often clean EEG recordings with assistance from independent component analysis (ICA), since it can decompose EEG recordings into a number of artifact-related and event-related potential (ERP)-related independent components. However, existing ICA-based artifact identification strategies mostly restrict themselves to a subset of artifacts, e.g., identifying eye movement artifacts only, and have not been shown to reliably identify artifacts caused by nonbiological origins like high-impedance electrodes. In this paper, we propose an automatic algorithm for the identification of general artifacts. The proposed algorithm consists of two parts: 1) an event-related feature-based clustering algorithm used to identify artifacts which have physiological origins; and 2) the electrode-scalp impedance information employed for identifying nonbiological artifacts. The results on EEG data collected from ten subjects show that our algorithm can effectively detect, separate, and remove both physiological and nonbiological artifacts. Qualitative evaluation of the reconstructed EEG signals demonstrates that our proposed method can effectively enhance the signal quality, especially the quality of ERPs, even for those that barely display ERPs in the raw EEG. The performance results also show that our proposed method can effectively identify artifacts and subsequently enhance the classification accuracies compared to four commonly used automatic artifact removal methods.**

***Index Terms*—Electrode-scalp impedance, electroencephalography (EEG), event-related potential (ERP), hierarchical clustering, independent component analysis (ICA).**

I. Introduction

BECAUSE of its high temporal resolution, electroencephalographic (EEG) recordings have been widely used to measure background activities of the brain as well as the specific activity for a cognitive task in brain–computer interface (BCI) [1]. However, a major problem of EEG recordings is that they are highly susceptible to various artifacts. In other words, it is almost impossible to see any event-related potential (ERP), the typical electrophysiological response to an internal or external stimulus, in the raw EEG recordings due to the presence of artifacts. However, neuroscientists are often interested in visualizing the signals and their time-domain ERPs such as N200 (a negative peak around 200 ms after the excitation due to the stimuli) or P300 (a positive peak around 300 ms after the excitation due to the stimuli) [2], [3]. Therefore, artifact identification and rejection is a crucial step in the ERP-related EEG-based BCI.

The artifacts can be divided into two categories: physiological and nonbiological artifacts, based on their origins. Physiological artifacts arise from biological sources other than the brain such as eye blinking, eye movements or muscle movements, etc. Nonbiological artifacts originate from outside the body due to factors such as high-impedance electrodes [4].

Over past decades, several approaches have been proposed to identify and remove these artifacts, especially for the physiological artifacts. The most trivial of these approaches involves simply deleting the portions of the data in which the EEG activity exceeds some predefined thresholds. However, this may lead to a large loss of data, which in turn could mean the loss of relevant recorded ERP signals [5]. Alternatively, regression methods have been implemented for artifact removal either in the time domain or frequency domain, particularly for the artifacts caused by eye blinks and eye movements. However, the performance of the regression methods depends on having a good reference signal [6]. Moreover, for muscle artifacts and nonbiological artifacts, for which it is difficult to find a suitable reference signal, regression methods are not applicable [7].

Recently, independent component analysis (ICA) has been a successful approach for artifact identification and removal. ICA is a statistical tool that decomposes a multichannel EEG recording into a set of independent components (ICs), which represent a statistical estimate of the maximally independent source signals [8]. Previous investigations have successfully demonstrated that ICA can separate multichannel EEG signals into brain-related and artifact-related ICs [6], [9], [10]. The key issue is efficient identification of artifact-related ICs. A number of different approaches have been proposed to guide this process, such as visual inspection based on researcher's prior knowledge of topographic patterns [6] and time-domain patterns [11]. However, these manual inspections require expert and well-trained staff.

Manuscript received April 9, 2014; revised October 14, 2014 and September 2, 2014; accepted November 4, 2014. Date of publication November 13, 2014; date of current version December 31, 2015. This work was supported by the Semiconductor Research Corporation, task # 1836.103 through the Texas Analog Center of Excellence (TxACE).

The authors are with the Department of Electrical Engineering, University of Texas at Dallas, Richardson, TX 75080 USA (e-mail: zouy@utdallas.edu; viswamnathan@utdallas.edu; rjafari@utdallas.edu).

Color versions of one or more of the figures in this paper are available online at http://ieeexplore.ieee.org.

Digital Object Identifier 10.1109/JBHI.2014.2370646

(a) (b)

Fig. 1. (a) (Left) EEG data acquisition system B. (Right) P300 speller matrix with one row intensified.

Moreover, they are not applicable for online BCI applications. Therefore, automatic identification has become an attractive alternative. Clustering techniques have been mostly employed to automatically separate brain-related ICs from artifact-related ones based on some specific features extracted from each IC. Qi *et al.* presented a K-means clustering based on the similarity between every two components in a multitrial EEG analysis [12]. Patidar and Zouridakis [13] and Ashtiyani *et al.* [14] presented an automatic artifacts identification method based on fuzzy C-means clustering. Both K-means and fuzzy C-means clustering are iterative methods. They both require the target number of clusters *a priori* to terminate the clustering iterations. However, the target number of clusters is often unknown; therefore, for the sake of a fully automatic solution, hierarchical clustering is a better approach and is employed in our proposed approach. Based on the hierarchical clustering method, several different features used to distinguish artifacts from real brain signal have also been presented in the previous works. Nicolaou and Nasuto propose an artifact removal algorithm via hierarchical clustering based on automutual information [15]. Milanesi *et al.* utilize the pair-wise mutual information as a hierarchical clustering feature for EEG late potential selection [16], [17]. However, they do not consider features that would highlight target ERPs (e.g., the latency of the ERP patterns or the specific electrodes contributing to the ERPs) in the artifacts removal framework. For this reason, in our proposed approach, utilization of features that contribute to the desired ERPs will enhance the quality of the extracted ERP and facilitate the eventual classification process. A preliminary result of using ERP-related features and hierarchical clustering for physiological artifact removal in Go/Nogo task with a wet electrode recording system has been reported in [18].

A review of the existing literature did not reveal a systematic approach for general artifact identification. Most approaches have been shown to recognize and reject major physiological artifacts like eye movements or muscle movement, while the detection of nonbiological artifacts has been reported only in a few studies and none of them constitute a robust approach for a portable recording system.

Similar to physiological artifacts, nonbiological artifacts caused by high-impedance electrodes are also a significant source of artifacts in the EEG recordings. High electrode-scalp impedance can lead to distortions that are difficult to separate from the actual EEG recordings [19]. Therefore, in many existing EEG systems, electrode-scalp impedance is measured prior to data acquisition. In order to prevent signal distortions, the impedance at each electrode in contact with the scalp should be below 5 kΩ for wet electrodes and 500 kΩ for dry electrodes [19]. When the impedance is above these limits, it is an indication that there is poor connectivity between the electrode and the scalp. Currently, researchers reduce the impedance of the electrodes by injecting more gel in wet-electrode systems, for instance, or providing more pressure and adjusting the placement of the electrodes in dry-electrode systems. These adjustments are typically made prior to (or during) the data acquisition stage and can be very time consuming. Therefore, a time-efficient approach for high-impedance artifact removal is desired. Mognon *et al.* [7] and Nolan *et al.* [5] both developed an EEG artifact removal framework, which can identify multiple artifacts including nonbiological artifacts caused by high-impedance electrodes. They identified high-impedance artifacts using spatial features such as the channel's correlation coefficients based on the assumption that in a high-density electrode recording system (number of electrodes larger than 100), most electrodes should correlate highly with neighboring electrodes. Therefore, an electrode with high impedance value will likely have a low correlation with other electrodes. Both methods showed their results on a 128-electrode system. However, these features are not applicable for a portable low-density electrode recording system, which is more and more prominent in recent BCI applications. Previous studies [20], [21] have demonstrated a correlation between the electrode-scalp impedance and EEG signal quality. In [20], Ferree *et al.* showed that lower impedance between the electrodes and the scalp improves the quality of EEG signals and mitigates the noise. In another study, Kappenman and Luck showed that the electrode-scalp impedance measure enables the characterization of the ERP signal quality. They found that the low-frequency noise in the ERP signal increases at electrodes with a higher impedance compared to those with low impedance [21]. Inspired by the aforementioned works, the impedance information is utilized to identify the nonbiological artifacts in our proposed approach. A preliminary study that shows the relationship between the electrode-scalp impedance information and the artifact signals has been reported in [22].

Our proposed solution for identification and removal of general artifacts would be valuable for EEG researchers and BCI users. First, the methods proposed represent a unified solution for all types of artifacts and not just ones caused by physiological phenomena. Second, a practical method must be applicable without the need of time-consuming preparations at the time of the experiment. Third, there have been several recent advancements in circuit techniques for an EEG acquisition system, and this is a good opportunity to use these techniques in the signal processing stage for artifact identification and removal. Therefore, a generalized automatic ICA-based algorithm for identification of all artifact-related ICs in the EEG recordings is proposed here. The first step consists of decomposing the EEG recordings into ICs. Two types of artifact are then considered: First, electrode-scalp impedance information is utilized to distinguish the nonbiological artifact-related ICs from brain-related ones. Second, the ERP-related temporal, spatial, and spectral features are utilized to identify physiological artifacts.

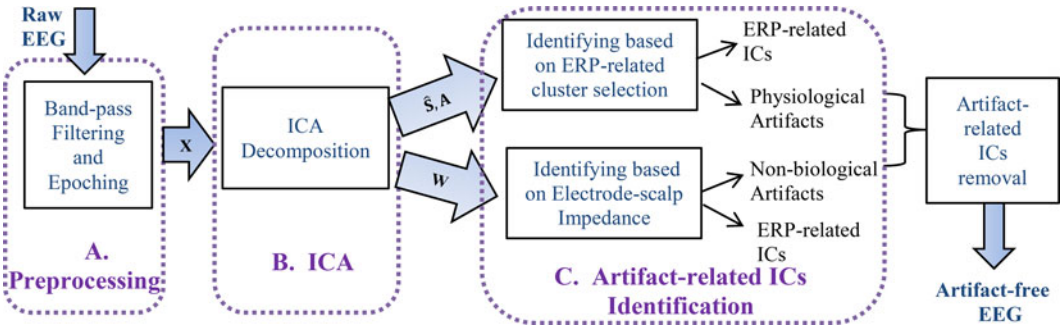

Fig. 2. Block diagram of the proposed automatic artifact identification and removal system.

This paper is organized as follows: Section II describes the experimental setup and Section III introduces the proposed automatic artifact-related ICs identification algorithm in detail. The experimental results are presented in Section IV. Finally, some conclusions are given in Section V.

II. Experimental Setup

A. Data Acquisition System

The data acquisition system is a custom platform designed and developed by our laboratory, shown in Fig. 1(a). It incorporates two daisy-chained TI ADS1299 analog front ends for EEG, a TI MSP430 microcontroller, and a BlueRadios dual mode Bluetooth radio for wireless communication of the data to a PC or any mobile device [23].

In order to measure the electrode-scalp impedance for each individual electrode, we use the "lead-off detection" feature of the TI ADS1299. A 24-nA sinusoidal ac current at a known frequency of 30.5 Hz is injected into each electrode (the lead-off detection technique is described in more detail in Section III). The sampling rate of our acquisition system is 250 Hz.

B. P300-Based BCI Task

The BCI application implemented in our study is the P300 speller introduced in [24]. It enables users to spell a word from a 6×6 matrix that includes all the letters of the alphabet as well as other useful symbols [see Fig. 1(b)]. The rows or columns intensify sequentially in a random order. To spell a word, the subjects are instructed to focus on the letter they wish to communicate by counting the number of times it intensifies. In response, a P300 evoked potential is elicited in the brain. This is a positive deflection in the EEG 300 ms after th stimulus is presented [24]. By identifying this P300 pattern, it is possible to infer the attended letter.

Ten healthy subjects participated in the experiment. They had no previous experience with the P300 speller task. Eight dry electrodes were placed at Fz, Cz, P3, Pz, P4, Oz, PO7, and PO8 using the international 10–20 system and a wet patch electrode was placed at the right mastoid and used as the reference. For each subject, two to five sessions of data were recorded. In each session, the subject was instructed to choose between 20 and 30 letters. Before each P300 session, a 30-s electrode-scalp impedance measurement was recorded. In order to emulate real-life scenarios of different impedances between each electrode and the scalp, no extra efforts were made to adjust the locations and connectivity of the cap and electrodes in the initial setup.

III. Method

The main steps in our proposed automatic artifact identification algorithm are illustrated in the scheme of Fig. 2 and described as follows:

A. EEG Data Preprocessing

Raw EEG recordings were bandpass filtered from 0.5 to 50 Hz. Epochs of 800-ms duration were extracted starting from the onset of the first row/column intensification.

B. Independent Component Analysis

ICA is a well-known statistical technique in signal processing literature that aims at finding linear projections of the data that maximize their mutual independence [25]. It is assumed that we observe an array of electrodes that provide a vector of N electrode recordings $\boldsymbol{v} = [v_1, v_2, \ldots, v_N]^T$ that are linear combinations of M unknown and statistically independent sources $\boldsymbol{s} = [s_1, s_2, \ldots, s_N]^T$. The objective of the ICA algorithm is to find a separating matrix W, such that

$$\boldsymbol{s} = W \times \boldsymbol{v}. \tag{1}$$

When applying the ICA to the EEG recordings, the resulting ICs represent the brain-related sources as well as artifact-related sources. This makes the ICA an effective solution for identifying the artifacts. Several ICA algorithms have been implemented and are publicly available. In this paper, we used the FastICA module of the EEGLAB toolbox [26] to decompose each EEG epoch into ICs. Each epoch consisted of eight components (corresponding to the eight EEG electrodes).

C. Artifact-Related IC Identification

After the ICA decomposition, we chose to leverage some well-known features in order to best capture the behavior of the ICs associated with the two different artifact classes. Here, we describe the features used for each artifact class.

1) Physiological Artifact-Related ICs:

a) Feature extraction: Eye blinks, eye movements and muscle movements are the major sources of physiological artifacts. In order to distinguish these artifacts from real brain signals, four kinds of features are extracted here:

1) *Temporal features:* Due to the presence of physiological artifacts like eye blinks, the amplitude of the artifact-related ICs will abruptly jump and show different temporal patterns compared to the normal brain-related ICs. This jump can be well captured by the *kurtosis* [27], which characterizes the relative peakedness of the amplitude distribution [28]. For example, ICs with eye blink artifacts exhibit relatively high kurtosis [27]. However, the slow amplitude drifts on the entire signal will also generate high kurtosis and hamper the detection of artifacts. Therefore, the whole IC is normalized to have zero mean before the calculation of kurtosis as in [7]

$$f_{\text{temporal}} = \frac{avg\_ep(s_i^4)}{avg\_ep((s_i^2)^2)} - 3 \tag{2}$$

where s_i indicates the time course of IC as defined in (1) of epoch *i*. *avg_ep* indicates the average within epoch *i* after mean removal.

2) *Spatial features:* The artifact-related ICs and the brain-related ICs are projected on different groups of electrodes. For instance, in our P300 experiment, the brain-related ICs are concentrated on the frontal and central electrodes (around Fz channel), while the eye blinks project most strongly on the far frontal site on the scalp [2]. To capture the spatial topography of artifact-related ICs, the *median* of each IC's topography weight is utilized here

$$f_{\text{spatial}} = \text{median}([a\,(1)_i\,, a\,(2)_i\,, \ldots, a\,(n)_i]) \tag{3}$$

where $a\,(n)$ is the IC topography weight matrix *A* ($A = W^{-1}$) at column *n* (for electrode *n*). In order to scale the topography weight for each electrode to the same range, a normalization process is implemented on $a\,(n)$ by dividing the square root of the sum of squares of $a\,(n)$ for all electrodes [7].

3) *Spectral features:* The normal power of EEG signals are in delta band (0–4 Hz), theta band (4–8 Hz), alpha band (8–13 Hz), and beta band (13–30 Hz) and most of it falls in the range of 1–20 Hz [29]. However, the artifacts show dissimilar power distribution. For example, the spectrum of muscle artifacts is characterized usually by a high value in the 20–50 Hz range [30]. These differences can be highlighted by the *average band power* of delta, theta, alpha, beta and gamma bands (gamma is 30–50 Hz)

$$\begin{aligned} f_{\text{spectral}} = \; & [F\,(\text{delta})\,F\,(\text{theta})\,F\,(\text{alpha}) \\ & F\,(\text{beta})\,F\,(\text{gamma})] \end{aligned} \tag{4}$$

where *F()* is the average band power which is calculated using MATLAB's pwelch function.

4) *Similarity over epochs:* The artifacts are random, unexpected, and usually only occur in some epochs. Thus, the epochs that contain artifacts have no common pattern and exhibit very low similarity with other epochs.

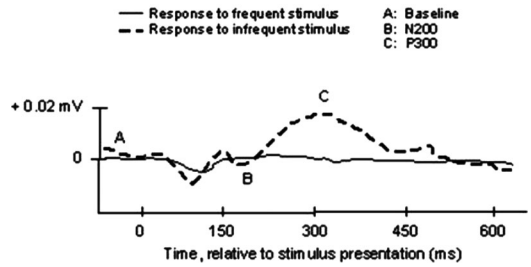

Fig. 3. Example of EEG signals with N200 and P300 patterns for target (infrequent stimulus) and nontarget (frequent stimulus) epochs [3].

On the other hand, the epochs with ERP-related ICs exhibit higher similarity with others. The correlation value is adopted to measure the similarity

$$f_{\text{similarity}} = \frac{\sum_{m=1, m\neq i}^{N_{ep}} r_{s_i, s_m}}{N_{ep} - 1} \tag{5}$$

where r_{s_i, s_m} is the correlation coefficient between ICs (s_i and s_m) calculated from epoch *i* and *m*. N_{ep} is the total number of epochs in the dataset.

Overall, an 8-D feature vector (one temporal feature, one spatial feature, five spectral features, and one similarity feature) is extracted from each IC.

b) Hierarchical clustering: In order to automatically distinguish artifact-related ICs from brain-related ICs, a hierarchical clustering approach based on the features described in the previous section is employed here. We choose the hierarchical clustering approach for two reasons: First, the dendrogram in the hierarchical clustering not only encapsulates the grouping for clusters, but also provides information on the closeness of the elements in each cluster in the form of the height of the node. Second, the entire clustering procedure can be accomplished without determining the number of clusters *a priori*.

c) Physiological artifacts identification: Since the physiological artifacts can randomly occur and are unexpected, it is difficult to generate a global model to identify them. Thus, instead of constructing a global template for artifact-related ICs, our approach is based on a global pattern that encapsulates models for signals of interest and identifies the artifact-related ICs by searching for the minimal contribution to this model. Neuroscientists have found that, for the P300 speller task, most ERP-related ICs have two common significant ERP patterns: N200 and P300 [2]. The cognitive representation of N200 is related to response inhibition and error-related negativity and the latency of N200 is related to the subject's health conditions (there is an increase in latency for subjects with psychiatric disorders), while the cognitive representation of P300 is related to the process of decision making and the latency of P300 depends on the complexity of the stimuli (the latency is longer during difficult stimulus tasks) [3], [31]. Fig. 3 shows an example of EEG signals with N200 and P300 patterns for target (infrequent stimulus) and nontarget (frequent stimulus) epochs [3]. A target epoch corresponds to the intensification of a row/column

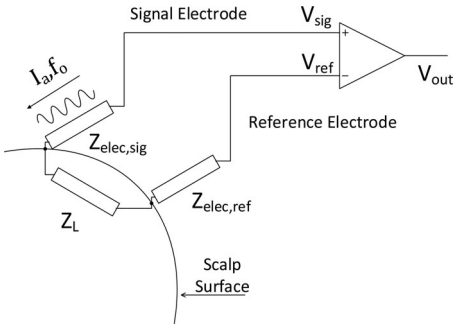

Fig. 4. Injecting current into the signal electrode for impedance measurement.

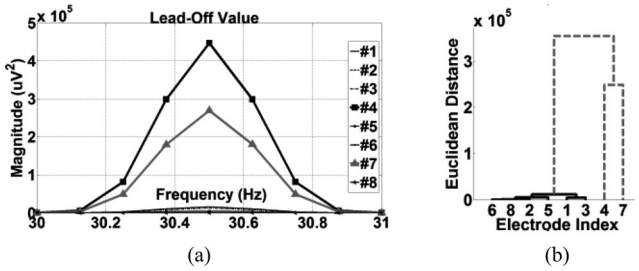

Fig. 5. (a) Electrode-scalp impedance for all electrodes. (b) Dendrogram plot after clustering for all electrodes' impedance on subject #1.

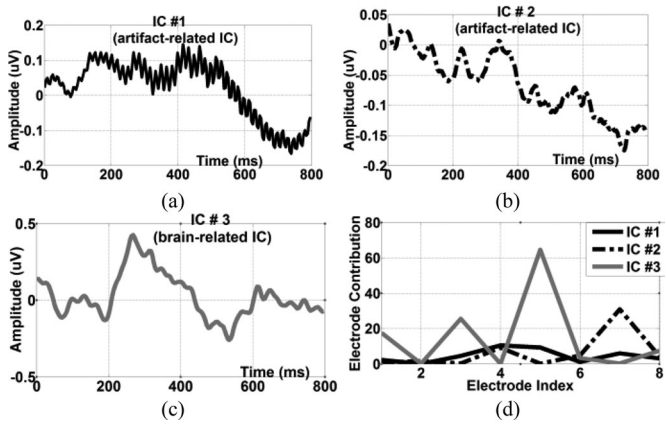

Fig. 6. (a)–(c) Three ICs generated from Subject #1. IC #1 (a) and #2 (b) are the artifact-related ICs. IC #3 (c) is the brain-related IC since it follows the ERP-related N200-P300 patterns. (d) Contribution of the electrodes in the ICs for Subject # 1.

including the desired letter, and a nontarget related to intensifications not including the desired letter.

Hence, we build a template to guide the artifact identification for all the subjects based on this *a priori* knowledge:

Step 1: Calculate the back-projection value p_i of each IC as follows:

$$p_i = W^{-1}(i) \times s_i \tag{6}$$

where p_i is the back-projection value of IC *i*, and $W^{-1}$is the inverse of the unmixing matrix.

Step 2: Calculate contribution of each cluster to the desired signal of interest patterns: N200 ($\emptyset_j^{n2}$) and P300 ($\emptyset_j^{P3}$), separately, since they have different cognitive representations and impact factors related to the latency. The contribution value $\phi_{\rm j}$ [see (7) and (8)] for each cluster is obtained by the average value p_i of all ICs in the cluster, which is then averaged over a specified time range:

$$\emptyset_j^{P3} = \frac{1}{t_{P3}^+ - t_{p3}^-}\left[\sum_{t_{P3}^-}^{t_{P3}^+}\left(\frac{1}{m}\sum_{i=1}^{m} p_i(t)\right)\right] \tag{7}$$

$$\emptyset_j^{n2} = \frac{1}{t_{n2}^+ - t_{n2}^-}\left[\sum_{t_{n2}^-}^{t_{n2}^+}\left(\frac{1}{m}\sum_{i=1}^{m} p_i(t)\right)\right] \tag{8}$$

where $\emptyset_j^{P3}$is the contribution value for the desired ERP (P300) of cluster *j*, $\emptyset_j^{n2}$ is the contribution value for N200, and *m* is the total number of components included in the cluster *j*. t_{n2}^- and t_{n2}^+ specify the latency range for the N200 pattern and t_{P3}^- and t_{P3}^+ specify the latency range for the P300 pattern. In our study, all subjects are between 20 and 30 with no history of psychiatric disorders and given the same stimuli and experimental orders; therefore, we use the same latency range: $t_{n2}^- = 200$ ms, $t_{n2}^+ = 300$ ms, $t_{p3}^- = 300$ ms, $t_{P3}^+ = 500$ ms for all the subjects.

Step 3: Finally, the cluster *j* which minimizes the difference between $\emptyset_j^{P3}$ and $\emptyset_j^{n2}$ is identified as being affected by artifacts and the ICs inside of this cluster are marked as artifact-related ICs.

2) Nonbiological Artifact-Related ICs: Poor scalp contact for a particular electrode that will produce consistently bad data for a long duration is the major source for nonbiological artifacts. The poor contact may be due to the drying out of gels used to establish a conductive path from the electrode to the scalp in a wet-electrode acquisition system or due to sweat, hair or the half-cell effect interfering with the connectivity between the scalp and the electrode for a dry-electrode system [32]. In order to identify this class of artifacts, the electrode-scalp impedance information is employed to guide the nonbiological artifact-related IC identification process.

a) Electrode-scalp impedance: Accurate measurement of EEG relies heavily on a low-impedance conductive path from the scalp to the signal acquisition device. If there is any disruption between an electrode and the scalp, the reported results may not be accurate. Typically, the contact quality of an electrode to the scalp is evaluated by the impedance value between the electrode and the scalp. One method to measure the electrode-scalp impedance would be to inject a current at the signal electrode, shown as I_a in Fig. 4. This technique is called "lead-off detection" and is provided on the TI ADS1299. When the applied current is a sinusoid at a known frequency f_o, then we have

$$V_{\text{out},f_0} = I_{a,f_0} \times Z_{\text{overall}}. \tag{9}$$

The frequency response of V_{out} at f_o is dominated by the voltage drop across the overall impedance of the circuit due to the injected current, I_a:

$$Z_{\text{overall}} = Z_{\text{elec,sig}} + Z_L + Z_{\text{elec,ref}}. \tag{10}$$

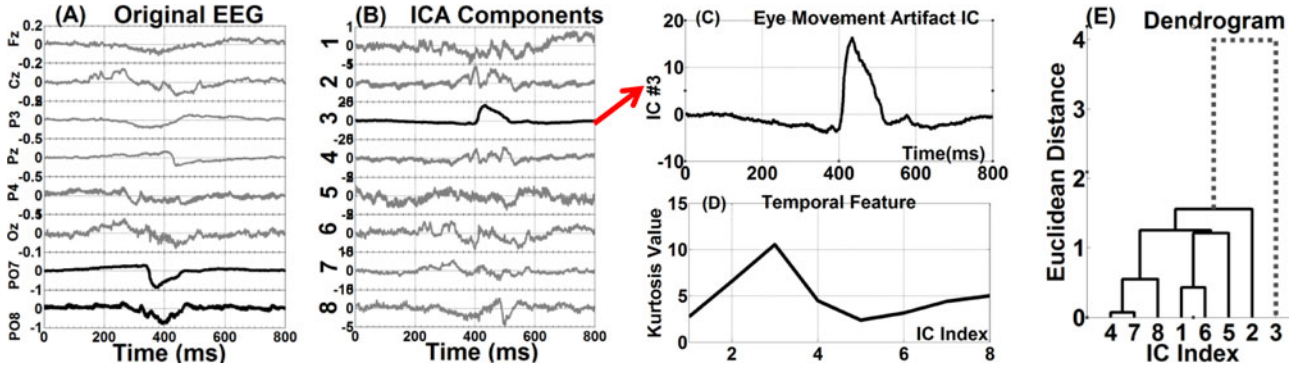

Fig. 7. Demonstration of eye movement artifact identified by ICA with temporal feature. (a) Epoch of 800-ms raw EEG data containing eye movement artifacts. (b) Corresponding ICA components. (c) IC#3 with abrupt jumps on the amplitude is identified as eye movement. (d) Temporal feature (kurtosis value) of all eight ICs. (e) Dendrogram plot after hierarchical clustering.

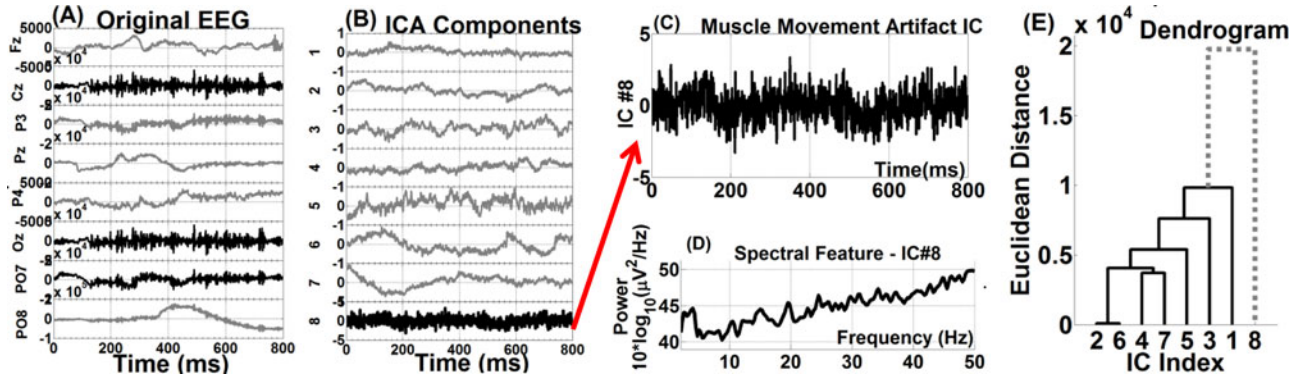

Fig. 8. Demonstration of muscle artifact identified by ICA with spectral feature. (a) Epoch of 800-ms raw EEG data containing muscle artifacts. (b) Corresponding ICA components. (c) Muscle artifact IC. (d) Abnormal spectral distribution of the muscle artifact IC. (e) Dendrogram plot after hierarchical clustering.

The overall impedance Z_{overall} is the combination of $Z_{\text{elec,sig}}$ (the impedance faced by the dry signal electrodes), Z_L (the impedance of the length of the scalp between two electrodes), and $Z_{\text{elec,ref}}$ (the impedance faced by the wet reference electrode). The power spectrum of the signal V_{out} at f_o is directly proportional to the impedance faced by the constant current I_a.

If the electrodes are properly connected with the scalp, the injected signal has minimal impact on V_{out}. However, when the contact quality becomes weak, the impedance $Z_{\text{elec,sig}}$ increases. Since the impedances Z_L and $Z_{\text{elec,ref}}$ remain relatively constant for all the electrodes during our experiments, any changes in the overall impedance Z_{overall} will be due to the various impedances of the dry electrodes and these will be reflected in frequency response of V_{out} at the frequency f_o in each channel. This gives us a measure of the relative impedances of the eight signal electrodes.

b) Nonbiological artifacts identification: In our study, we inject a sinusoidal signal with $f_o = 30.5$ Hz as the constant current I_a and compute the magnitude of the power spectra of the output signals at 30.5 Hz as a measure of the impedance between the electrode and the scalp. A higher magnitude at 30.5 Hz, measured at one output channel, implies higher impedance faced by the corresponding electrode and therefore poorer contact between that electrode and the scalp. Fig. 5(a) shows the magnitude of the power spectra between 25 and 35 Hz for the signal originating from each electrode for subject #1. Among all the electrodes, electrodes #4 (Pz) and #7 (PO7) exhibit extremely high magnitude at 30.5 Hz.

In order to separate electrodes (#4 and #7) which show much higher impedance compared to the other electrodes, a Euclidean distance-based hierarchical clustering procedure is employed on the magnitude values at 30.5 Hz. Fig. 5(b) shows the dendrogram plot of eight electrodes on subject #1. After the clustering process, electrodes #4 and #7 which show higher impedance values in Fig. 5(b) are grouped together and separated from the other six electrodes.

We then transform the vector multiplication in (1) and represent it as a linear combination:

$$\hat{s}_i = \sum_{j=1}^{N} w_{ij} \times v_j \tag{11}$$

where *i* is the IC index number and *j* is the electrode index number. w_{ij} is the *ij*th element of the unmixing matrix *W*. Each IC $\hat{s}_i$ consists of all the electrodes, and each electrode has its own contribution w_{ij}. These ICs represent the brain-related potentials as well as artifacts. In our study, the brain-related potentials should

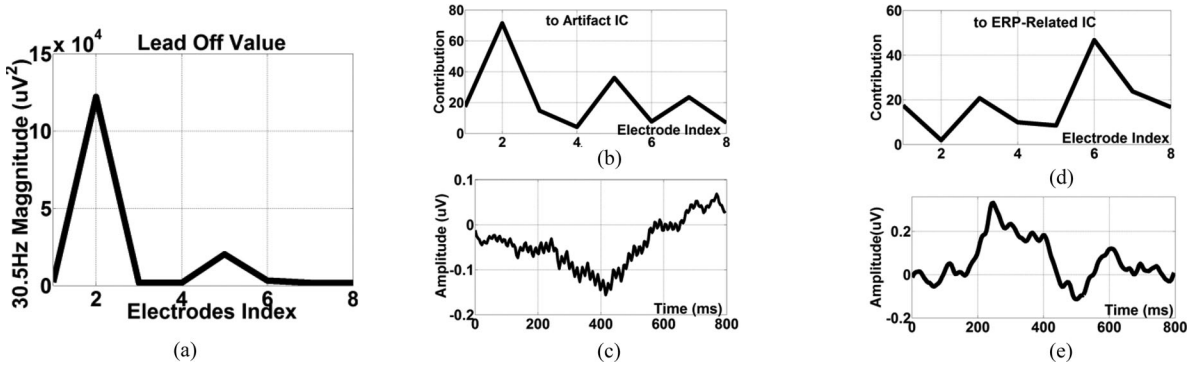

Fig. 9. Demonstration of nonbiological artifact identified by ICA with lead-off value: (a) Lead-off value for eight electrodes. (b) Eight electrodes' contribution to artifact-related IC. (c) Artifact-related IC. (d) Eight electrodes' contribution to the ERP-related IC. (e) ERP-related IC.

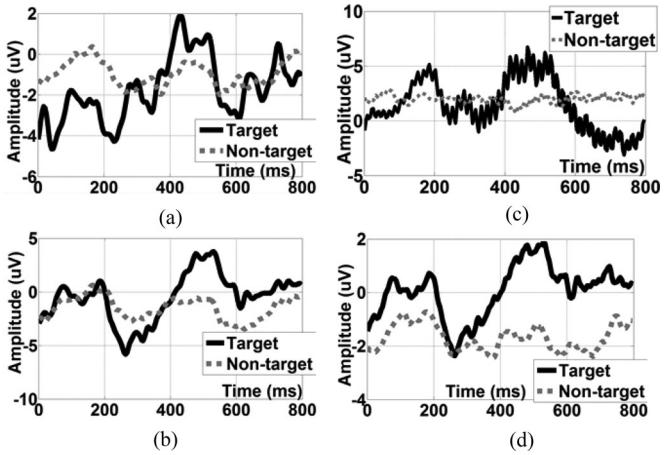

Fig. 10. (a) Original EEG signals and (b) artifact-free EEG signals for the case that the original signals show visible N200-P300. Both exhibit the N200-P300 complex, but the complex becomes more prominent after application of our proposed algorithm. (c) Original EEG signals and (d) artifact-free EEG signals for the case that the original signals do not exhibit the N200-P300 complex. The artifact-free signals clearly show the N200-P300 complex.

contain two patterns: N200 and P300 (see Fig. 3). Therefore, IC #3 in Fig. 6(a) can be classified as ERP-related IC since it follows these two patterns, and IC #1 [see Fig. 6(b)] and #2 [see Fig. 6(c)] are artifact-related ICs.

The contribution of each electrode to the above ICs is shown in Fig. 6(d). After comparing the different contributions of each electrode, we can see that for the artifact-related ICs (IC #1 and IC #2), electrodes #4 and #7, which have higher impedance value, provide the maximal contributions. However, for the ERP-related IC (IC#3), these two high-impedance electrodes have minimal contributions.

Based on the relationship between the impedance and the contribution of each individual electrode to the ICs, the nonbiological artifacts can be identified in the following steps:

Step 1: Calculate the electrode-scalp impedance for each individual electrode and employ the clustering technique to find the electrodes which show extremely high impedance compared to others.

Step 2: Compare the contributions of all the electrodes for each IC. The ICs that represent the nonbiological artifacts should satisfy the following condition: the electrodes which have maximal impedance values provide the maximal contributions to this IC. If this condition is satisfied, the corresponding ICs are identified as artifact-related ICs.

D. Artifacts Removal and Clean EEG Reconstruction

In the last step, the components labeled as artifact-related ICs are removed from the data. Then, the artifact-free EEG data was reconstructed from the remaining ICs.

IV. Results

A. Physiological Artifacts Identification

1) Example 1: Eye Movement Artifacts Identification: Fig. 7(a) shows an epoch of 800 ms of the original EEG data collected from eight electrodes. Around 400 ms, eye movement artifacts are observed on the signals of electrodes PO7 and PO8. The corresponding ICA components are shown in Fig. 7(b). IC#3 is automatically identified as eye movement artifacts since its amplitude abruptly jumps, as shown in Fig. 7(c). This jump is captured by the temporal feature, kurtosis value. Fig. 7(d) shows the kurtosis value for all eight ICs and IC#3 shows a very high value. Fig. 7(e) shows the dendrogram plot of eight ICs after hierarchical clustering using the temporal feature. After the clustering, IC#3 is isolated from the other ICs.

2) Example 2: Muscle Artifacts Identification: Fig. 8 demonstrates the identification of muscle artifacts by ICA using spectral features. It shows another epoch of 800 ms of the original EEG data [see Fig. 8(a)] and its ICA components [see Fig. 8(b)]. The artifacts occurring during the entire epoch of the signals from channels Cz, Oz, and PO7 [see Fig. 8(a)] are isolated to ICA component 8 [see Fig. 8(c)]. IC#8 is automatically identified as muscle artifacts due to its abnormal spectral distribution that shows very high value in the 20–50 Hz range [see Fig. 8(d)]. Fig. 8(e) shows the dendrogram plot of eight ICs after hierarchical clustering using the spectral feature. After the clustering, IC#8 is separated from the other ICs.

B. Nonbiological Artifacts Identification

Fig. 9 demonstrates the identification of nonbiological artifacts by ICA using the lead-off value. Fig. 9(a) shows the lead-off value (magnitude at 30.5 Hz) of eight electrodes. Electrode #2 shows an extremely high value compared to other electrodes. Fig. 9(b) shows the contributions from each electrode to an IC [shown in Fig. 9(c)]. This IC receives maximal contribution from electrode #2. Since electrode #2 has the highest lead-off value, the IC shown in Fig. 9(c) is automatically identified as artifact-related. On the other hand, Fig. 9(d) shows the contributions from each electrode to another IC [shown in Fig. 9(e)]. This IC receives minimal contribution from electrode #2. Since the ERP-related component should have minimal relationship with electrodes that show high impedance, the IC shown in Fig. 9(e) is identified as ERP-related IC.

C. Performance Evaluation by Reviewing Reconstructed Artifact-Free EEG

Next, we compare the original EEG recordings with the reconstructed EEG to evaluate the performance of our algorithm on signal quality enhancement, especially ERP-related information enhancement. In order to better evaluate the performance, we separated the ten subjects into two groups. The four of them that showed visible desired ERP-related patterns (N200 and P300) in the original EEG recordings are in group 1. The other six subjects who had no visible ERP-related patterns are in group 2.

1) Group 1: Visible ERP Patterns Exist in the Original EEG Recordings: Fig 10(a) and (b) shows the comparison result of one subject who shows visible ERPs in the original EEG recordings. The original EEG signals are shown in (a) and the signals after applying our automatic artifact identification and removal algorithm are shown in (b). As indicated in Fig. 10(b), after artifact removal procedure, the N200-P300 complex is more prominent than in the original EEG signals.

2) Group 2: No Visible ERP Patterns Exist in the Original EEG Recordings: Fig 10(c) and (d) depicts the comparison result for another subject who barely shows visible ERPs in the original EEG recording. As shown in (c), the N200-P300 complex is not visible before artifact removal. However, after artifact removal by the proposed algorithm, a view of N200-P300 complex is clearly recognizable on the reconstructed signals in Fig. 10(d). It demonstrates that the proposed algorithm can effectively extract the ERP-related information even when there are no clearly visible ERPs in the original signals.

These results illustrate the effectiveness of our proposed algorithm in identifying and removing artifacts. More importantly, our algorithm can also highlight ERP-related information in the resulting artifact-free signals and distinguish the target and nontarget epochs.

D. Performance Evaluation by Classification Accuracy Comparison With Alternate Methods

Finally, we evaluate the performance of our proposed artifacts identification and removal algorithm by comparing the classification accuracies (target epochs versus nontarget epochs) with four commonly used automatic artifact identification and removal methods. The proposed approach outperforms method 1 that uses k-means clustering based on the similarity [12] (shown in Column #2 of Table I) and method 2 that uses hierarchical clustering based on automutual information [15] (shown in Column #3 of Table I). It is due to the fact that these two methods are only suitable for the physiological artifacts and could not identify nonbiological artifacts. The ADJUST [7] (shown in Column #4 of Table I) and FASTER [5] (shown in Column #5 of Table I) methods can achieve better performance than the previous two methods since they consider the nonbiological artifacts in their artifact identification process. However, the accuracies obtained by our proposed method are higher than these two methods since our approach is more applicable for the low-density electrode system. We also conducted the statistical t-test, shown on the last row of Table I, to evaluate the significance of the improvements between our algorithm and the other four algorithms. All t-tests resulted in a p-value less than 0.05 which indicates that the improvement in accuracy is statistically significant.

TABLE I
CLASSIFICATION ACCURACY (IN %) ACHIEVED BY FOUR COMMONLY USED AUTOMATIC ARTIFACT IDENTIFICATION AND REMOVAL METHODS VERSUS OUR PROPOSED METHOD

subject	K-means with similarity [12]	Auto-mutual information [15]	ADJUST [7]	FASTER [5]	**Our Method**
#1	84.8	86.3	88.7	89.9	**92.1**
#2	70.9	72.1	73.4	73.5	**76.6**
#3	76.2	74.5	79.6	79.9	**83.5**
#4	69.5	70.2	73.5	72.9	**77.8**
#5	75.5	74.5	76.9	77.5	**80.9**
#6	74.2	73.9	77.5	78.1	**82.9**
#7	75.2	74.2	78.9	78.4	**84.4**
#8	75.9	77.1	80.6	79.3	**85.2**
#9	81.7	81.1	83.3	83.7	**86.4**
#10	82.9	83.6	85.9	85.6	**89.4**
Avg.	*76.68*	*76.75*	*79.83*	*79.88*	***83.92***
p-value	*<0.01*	*<0.01*	*<0.05*	*<0.05*	

V. CONCLUSION

A novel automated artifact-related ICs identification algorithm has been presented in this paper. The proposed methods take into account both physiological artifacts and nonbiological artifacts. An ERP-related clustering method is proposed for physiological artifact-related ICs identification. A quantitative comparison of original EEG signals with reconstructed artifact-free signals shows that the proposed algorithm can effectively enhance the ERP quality for all subjects in the study, even for those that barely display ERPs in the original recordings. Electrode-scalp impedance information was employed for nonbiological artifact-related ICs identification. Quantitative comparisons of the proposed algorithm to other methods show that significant performance improvements were achieved using our proposed method compared to four commonly used automatic removal methods for noisy ICs.

REFERENCES

[1] E. Niedermeyer and F. L. da Silva, *Electroencephalography: Basic Principles, Clinical Applications, and Related Fields*. Baltimore, MD, USA: Williams & Wilkins, 2005.

[2] M. Falkenstein, J. Hoormann, and J. Hohnsbein, "ERP components in go/nogo tasks and their relation to inhibition," *Acta psychologica*, vol. 101, no. 2, pp. 267–291, 1999.

[3] S. H. Patel and P. N. Azzam, "Characterization of n200 and p300: Selected studies of the event-related potential," *Int. J. Med. Sci.*, vol. 2, no. 4, pp. 147–154, 2005.

[4] M. Fatourechi, A. Bashashati, R. K. Ward, and G. E. Birch, "EMG and EOG artifacts in brain computer interface systems: A survey," *Clin. Neurophysiol.*, vol. 118, no. 3, pp. 480–494, 2007.

[5] H. Nolan, R. Whelan, and R. Reilly, "FASTER: Fully automated statistical thresholding for EEG artifact rejection," *J. Neurosci. Methods*, vol. 192, no. 1, pp. 152–162, 2010.

[6] T.-P. Jung, S. Makeig, C. Humphries, T.-W. Lee, M. J. Mckeown, V. Iragui, and T. J. Sejnowski, "Removing electroencephalographic artifacts by blind source separation," *Psychophysiology*, vol. 37, no. 2, pp. 163–178, 2000.

[7] A. Mognon, J. Jovicich, L. Bruzzone, and M. Buiatti, "Adjust: An automatic EEG artifact detector based on the joint use of spatial and temporal features," *Psychophysiology*, vol. 48, no. 2, pp. 229–240, 2011.

[8] A. Hyvärinen and E. Oja, "Independent component analysis: Algorithms and applications," *Neural Netw.*, vol. 13, no. 4, pp. 411–430, 2000.

[9] T.-P. Jung, S. Makeig, M. Westerfield, J. Townsend, E. Courchesne, and T. J. Sejnowski, "Removal of eye activity artifacts from visual event-related potentials in normal and clinical subjects," *Clin. Neurophysiol.*, vol. 111, no. 10, pp. 1745–1758, 2000.

[10] S. Makeig, M. Westerfield, T.-P. Jung, S. Enghoff, J. Townsend, E. Courchesne, and T. Sejnowski, "Dynamic brain sources of visual evoked responses," *Science*, vol. 295, no. 5555, pp. 690–694, 2002.

[11] T.-P. Jung, S. Makeig, M. Westerfield, J. Townsend, E. Courchesne, and T. J. Sejnowski, "Analysis and visualization of single-trial event-related potentials," *Human Brain Mapping*, vol. 14, no. 3, pp. 166–185, 2001.

[12] H. Qi, Y. Zhu, D. Ming, B. Wan, Y. Wang, and R. Zhang, "Independent component automatic clustering and its application on multi-trails imaginary hand movement related EEG," in *Proc. IEEE Int. Conf. Virtual Environments, Human-Comput. Interfaces Meas. Syst.*, 2009, pp. 149–153.

[13] U. Patidar and G. Zouridakis, "A hybrid algorithm for artifact rejection in EEG recordings based on iterative ICA and fuzzy clustering," in *Proc. 30th Annu. Int. Conf. IEEE Eng. Med. Biol. Soc.*, 2008, pp. 50–53.

[14] M. Ashtiyani, S. Asadi, and P. M. Birgani, "ICA-based EEG classification using fuzzy c-mean algorithm," in *Proc. 3rd Int. Conf. Inf. Commun. Technol.: From Theory Appl.*, 2008, pp. 1–5.

[15] N. Nicolaou and S. J. Nasuto, "Automatic artefact removal from event-related potentials via clustering," *J. VLSI Signal Process. Syst. Signal, Image, Video Technol.*, vol. 48, nos. 1/2, pp. 173–183, 2007.

[16] M. Milanesi, C. James, N. Martini, A. Gemignani, D. Menicucci, B. Ghelarducci, and L. Landini, "Late positive event-related potentials enhancement through independent component analysis clustering," in *Proc. 4th IET Int. Conf. Adv. Med., Signal Inf. Process.*, 2008, pp. 1–4.

[17] M. Milanesi, C. James, N. Martini, D. Menicucci, A. Gemignani, B. Ghelarducci, and L. Landini, "Objective selection of EEG late potentials through residual dependence estimation of independent components," *Physiol. Meas.*, vol. 30, no. 8, pp. 779–794, 2009.

[18] Y. Zou, J. Hart, and R. Jafari, "Automatic EEG artifact removal based on ICA and hierarchical clustering," in *Proc. IEEE Int. Conf. Acoust., Speech Signal Process.*, 2012, pp. 649–652.

[19] M. Teplan, "Fundamentals of EEG measurement," *Meas. Sci. Rev.*, vol. 2, no. 2, pp. 1–11, 2002.

[20] T. C. Ferree, P. Luu, G. S. Russell, and D. M. Tucker, "Scalp electrode impedance, infection risk, and EEG data quality," *Clin. Neurophysiol.*, vol. 112, no. 3, pp. 536–544, 2001.

[21] E. S. Kappenman and S. J. Luck, "The effects of electrode impedance on data quality and statistical significance in ERP recordings," *Psychophysiology*, vol. 47, no. 5, pp. 888–904, 2010.

[22] Y. Zou, O. Dehzangi, V. Nathan, and R. Jafari, "Automatic removal of EEG artifacts using electrode-scalp impedance," in *Proc. IEEE Int. Conf. Acoust., Speech, Signal Process.*, 2014, pp. 2054–2058.

[23] V. Nathan, J. Wu, C. Zong, Y. Zou, O. Dehzangi, M. Reagor, and R. Jafari, "Demonstration paper: A 16-channel bluetooth enabled wearable EEG platform with dry-contact electrodes for brain computer interface," in *Proc. 4th Conf. Wireless Health*, 2013, p. 17.

[24] L. Farwell and E. Donchin, "Talking off the top of your head: Toward a mental prosthesis utilizing event-related brain potentials," *Electroencephalography Clin. Neurophysiol.*, vol. 70, no. 6, pp. 510–523, 1988.

[25] R. Vigário, J. Sarela, V. Jousmiki, M. Hamalainen, and E. Oja, "Independent component approach to the analysis of EEG and MEG recordings," *IEEE Trans. Biomed. Eng.*, vol. 47, no. 5, pp. 589–593, May 2000.

[26] A. Delorme and S. Makeig, "EEGLAB: An open source toolbox for analysis of single-trial EEG dynamics including independent component analysis," *J. Neurosci. Methods*, vol. 134, no. 1, pp. 9–21, 2004.

[27] A. Delorme, T. Sejnowski, and S. Makeig, "Enhanced detection of artifacts in EEG data using higher-order statistics and independent component analysis," *Neuroimage*, vol. 34, no. 4, pp. 1443–1449, 2007.

[28] D. G. Manolakis, V. K. Ingle, and S. M. Kogon, *Statistical and Adaptive Signal Processing: Spectral estimation, Signal Modeling, Adaptive Filtering, and Array Processing*, vol. 46. Norwood, MA, USA: Artech House, 2005.

[29] J. Malmivuo and R. Plonsey, *Bioelectromagnetism: Principles and Applications Of Bioelectric and Biomagnetic Fields*. New York, NY, USA: Oxford Univ. Press, 1995.

[30] S. Makeig and J. Onton, "ERP features and EEG dynamics: An ICA perspective," in *Oxford Handbook of Event-Related Potential Components*. New York, NY, USA: Oxford Univ. Press, 2009.

[31] S. Sur and V. Sinha, "Event-related potential: An overview," *Ind. Psychiatry J.*, vol. 18, no. 1, pp. 70–73, 2009.

[32] Y. M. Chi, T.-P. Jung, and G. Cauwenberghs, "Dry-contact and noncontact biopotential electrodes: Methodological review," *IEEE Rev. Biomed. Eng.*, vol. 3, pp. 106–119, 2010.

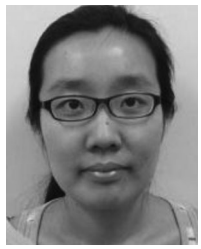

Yuan Zou (S'12) received the B.S. degree in electrical engineering from the Dalian University of Technology, Dalian, China, the M.Sc. degree in electrical engineering from Clarkson University, Potsdam, NY, USA, in 2007 and 2010, respectively. She is currently working toward the Ph.D. degree in electrical engineering at the University of Texas at Dallas, Richardson, TX, USA.

Her research interests include design and implementation of real-time digital signal processing systems and signal processing algorithm optimization applied to noninvasive brain–computer interface.

Viswam Nathan (S'13) received the B.S. degree in computer engineering from the University of Texas at Dallas, Richardson, TX, USA, in 2012, where he is currently working toward the Ph.D. degree in computer engineering.

His research interests include design and development of a wearable and reconfigurable dry electrode-based brain–computer interface as well as signal-processing techniques to assess the quality and reliability of the acquired signal.

Roozbeh Jafari (SM'12) received the Ph.D. degree in computer science from the University of California, Los Angeles, CA, USA, and completed a postdoctoral fellowship at University of California, Berkeley, CA.

He is currently an Associate Professor at the University of Texas at Dallas, Richardson, TX, USA. His research interests include the area of wearable computer design and signal processing. His research has been funded by the NSF, NIH, DoD (TATRC), AFRL, AFOSR, DARPA, SRC, and industry (Texas Instruments, Tektronix, Samsung & Telecom Italia). He has published more than 100 papers in refereed journals and conferences. He has served as the General Chair and Technical Program Committee Chair for several flagship conferences in the area of Wearable Computers including the ACM Wireless Health 2012 and 2013, International Conference on Body Sensor Networks 2011 and International Conference on Body Area Networks 2011.

Dr. Jafari is the recipient of the NSF CAREER Award (2012) and the RTAS 2011 Best Paper Award. He is an Associate Editor for the IEEE SENSORS JOURNAL, IEEE JOURNAL OF BIOMEDICAL AND HEALTH INFORMATICS, and IEEE INTERNET OF THINGS JOURNAL.